Chapter 4

Complex Langevin dynamics of spherical dimers

Much of the calibration theory discussed in Chapter 2 assumes that the target particle in question is a single sphere, one whose scattering and motion is easily computed. However, while working with dense colloidal suspensions, one often ends up trapping more than one sphere. Li and Arlt [12] studied the case of two microspheres trapped in a single OT and found that multiple trapped beads could be mistaken for a single trapped bead with altered trap stiffness (see **??**). Theoretical studies on the case of two trapped microspheres by Xu *et al.* [24] employed a ray-optics based model to show that the two trapped beads are brought into physical contact with each other by optical forces and they also calculated the axial equilibrium positions of the two trapped beads as a function of their size. Experiments in [14] confirmed that the two trapped beads indeed experience different trap stiffnesses in the vicinity of the same potential well.

There are further discussions looking into the dynamics of a whole host of asymmetrically shaped particles [13, 20, 8], their results all showing that predicting the behaviour an arbitrary shaped particle comes with great difficulty due to the fact that the optical force is dependent on a greater number of variables such as orientation and size factors.

With the initial goal of the project being to induce nucleation events via a rotating

sphere, the aim of this chapter is to - in a limited capacity simulate and investigate the influence of a second particle being bound to our target sphere. The choice of a dimer, instead of an amorphous solid that might better represent a growing crystalline solid, allows us to consider how the dynamics of the aggregate change by varying a single parameter, namely the size ratio of the two spheres. Additionally, attempting to simulate an amorphous aggregate is rather difficult as calculating the optical force and torque is computationally slow. We build upon the works of Vigilante *et al* [22] to consider asymmetric spherical dimers and how varying size parameters alters the dynamics and additionally makes characterising their interactions within an optical trap more cumbersome.

In this chapter we will consider how the addition of a second sphere changes the trapping dynamics by introducing multiple equilibrium positions. These positions are dependent on both the size ratio of the dimer and its orientation relative to the trap. This is important to address, for while the the dimers' diffusive behaviour is the same, regardless of position and orientation, how it interacts with the trap may produce the wildly different results. Furthermore, we look at how our dimers interact with circularly polarised light, this is especially pertinent as the original plan was to utilise circularly polarised light to generate fluid flow in a supersaturated solution. The rotational motion of dimers in circularly polarised light goes against much of the established literature and suggests that the transfer of spin angular momentum is enabled by combining particles together. And lastly, we demonstrate how a quadrant photo diode, performs in characterising the actual interactions between a dimer and the optical trap. We do so to demonstrate that much of the dimer's trajectory information is either lost or poorly described by simple calibration techniques, making their motion difficult to characterise.

4.0.1 Simulation Parameters

As a paradigmatic example, consider a dimer suspended in water ($n_p = 1.59, n_m = 1.33$) located at the focus of a Gaussian beam (more specifically a Laguerre-Gaussian beam of mode $[0, 0]$, see (**??**)), the beam is focused by a objective with numerical aperture

of 1.2 and is x polarised. The size ratio of the two spheres is given by $a_I/a_{II} = 2$ where a_I is kept at 1 μm unless specified otherwise; the dimer's orientation is given by a unit vector connecting the centres of both spheres (see **??**). We define the 'standard' orientation as being aligned with the direction of beam propagation direction - and therefore the 'inverted' orientation is defined when the dimer is orientated against the direction of beam orientation (see left hand side of figure 4.1).

4.1 Positional and Orientational dependence of Trapping forces

If we wanted to start from first principles and determine the trap strength on our target particle the first step would be to locate the equilibrium position relative to the trap focus. For a single sphere it is easy to enough to understand that its centre of mass will be drawn to focal point of the laser due to gradient forces, once there the force is analogous to a harmonic spring with a fixed trap stiffness (see fig.**??**). Now, if we consider instead a dimer, we now have two spheres both being drawn to the focus along by the same gradient force; in addition the scattering force is significantly more complex due to both spheres scattering the electromagnetic fields. This mutual scattering between individual spheres is what makes simulating spherical aggregates far more difficult compared to a single sphere, and even harder still to predict the position where the dimer's centre of mass is in equilibrium.

Because the scattering force is only significant in the direction of beam propagation [7] we can assume there will only be a single potential well lying at the centre of the beam. Along the beam axis, such an assumption is no longer valid due to fact that spherical aggregates experience inter-particle scattering. This is a key reason for using *mstm* as it accounts for that behaviour. The methodology for computing optical forces has been covered extensively for a number of different trapping conditions [15]. So it is relatively easy to compute the trapping force and determine the equilibrium position by finding the position that minimises the net optical force and the local gradient is negative ($\delta F/\delta x < 0$) - we can assume that for a dielectric sphere the optical torque is

negligible. For a dimer (or any arbitrary spherical aggregate), we now must consider both its position and orientation and find where the net optical force and torque are minimised.

After computing its T-matrix via *mstm* and supplying that to *ott* we compute the optical force exerted by a 50 mW laser via (**??**) in the axial direction while the dimer is in its 'standard' orientation. As expected we see a single point where the dimer will be in equilibrium, the linear fit in fig. 4.1(a) indicates a that the force can be modelled as a harmonic potential close to the equilibrium position ($F_z \approx -\kappa_z z$). The second point where the axial force goes to 0 cannot be considered as equilibrium position as the positive gradient indicates that the trap is unstable unless Brownian motion is ignored.

We repeated the same calculation but now while the dimer is in its 'inverted' orientation, instead of a single point where the optical force is minimised we see that there are instead two separate equilibrium positions, one above the focus and one below the focus. In this particular example the two positions are far enough apart that both can be considered as separate harmonic traps.

We can see that both equilibrium positions have comparable axial trap stiffness (κ_z), however the difference in the transverse trap stiffness (κ_x) is far more noticeable. The same dimer was trapped at each of the axial equilibrium positions and the transverse force was evaluated. While in all three cases the dimer can be trapped the linear range where that would typically associated with a stable trap is far narrower in the 'standard' orientation compared to the 'inverted' cases. This highlights one of the challenges involved with studying asymmetric particles, even though its a simple enough process to trap them they maybe characterised very differently depending on their relative position and orientation towards the focus. This can have a significant impact on rheological studies - or attempting to probe any local property - as the variance in trap strength can result in large errors over repeated measurements.

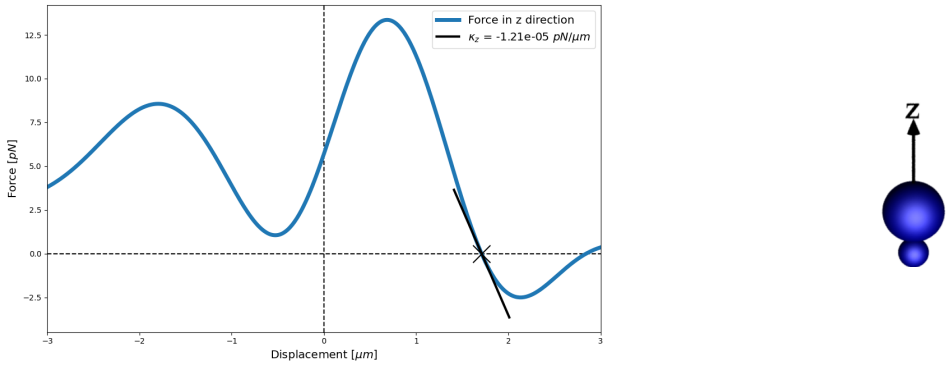

(a)

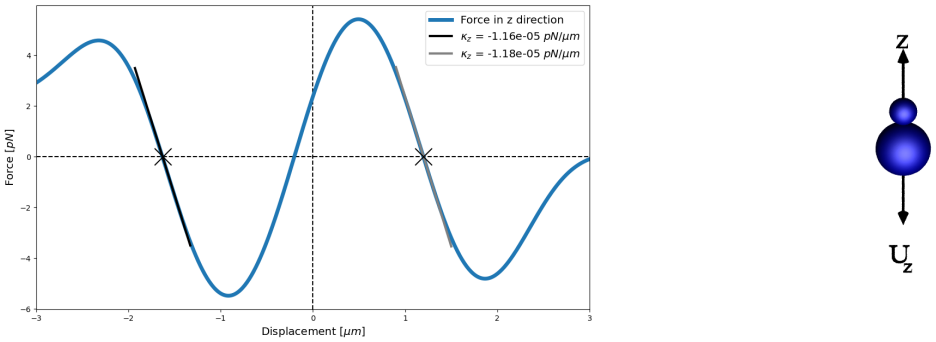

(b)

Figure 4.1: Plots of force vs displacement of the centre of mass of the dimer (µm) for the case of a dimer of size ratio 2. (a) is the case where the dimer is in its' 'standard' orientation, where the dimer is trapped at $z = 1.71\ \mu m$. (b) is the case where the dimer is in its' 'inverted' orientation, the dimer is trapped at two positions: $z = 1.20\ \mu m$ & $z = -1.63\ \mu m$. On the left are renders to visualise the dimer orientation are shown below each plot. The black lines on each force-curve is a linear fit with the slope being reported as the trap stiffness in the legend.

For completeness the harmonic traps were located for dimers across a range of size ratios - from $a_I/a_{II} = 1$ to $a_I/a_{II} = 10$ - while also recording the trap stiffness for each trap. The same simulation parameters are used here as for figures 4.1 & 4.2. As shown in Fig. 4.3 a_{II} decrease the dimer begins to approximate a single homogenous sphere - at least in terms of location and trap strength. However, for intermediate sized dimers (between $a_I/a_{II} = 1.1$ to $a_I/a_{II} = 4$), a second equilibrium position is found below the trapping focus. Previous work using the ray-optics model have confirmed even in the

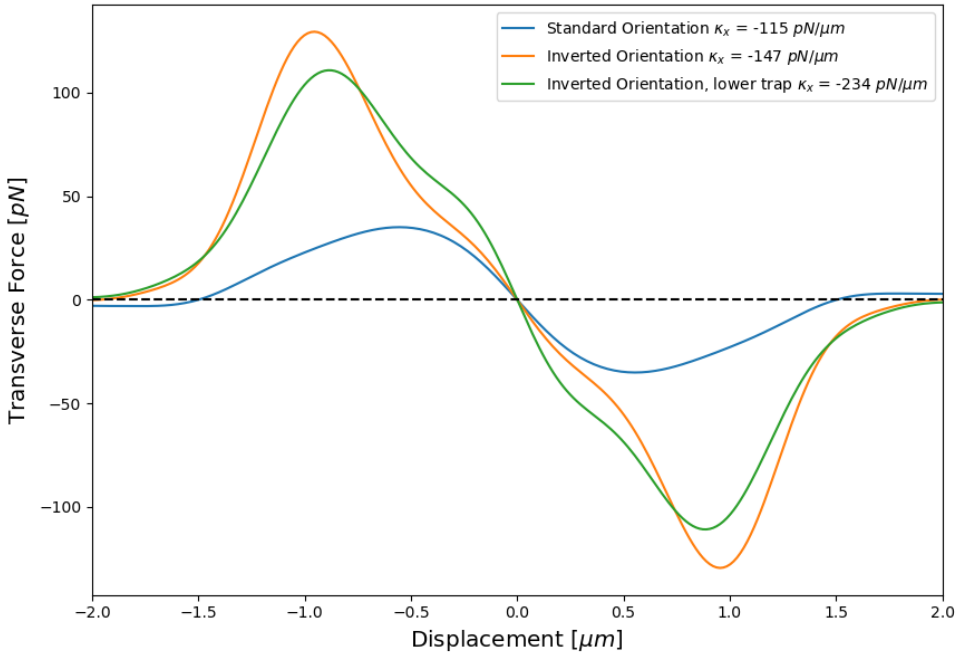

Figure 4.2: Plots of force vs displacement of the dimer's centre of mass spheres, where a positive force indicates the dimer is directed right on the x-axis, and vice versa for a negative force. The same simulation parameters are used here as in fig 4.1 (a) and (c). The blue curve representing the force response for a dimer in its standard orientation, orange being the inverted case, and green the same case but placed below the focus.

case that two spheres begin separated the electric field will align the particles as such that they make contact and are trapped together about a single trapping position [24]. Furthermore it has been shown through proper manipulation of the Gaussian or Bessel beam modes that any number of trapping potentials can be developed [19] for nanoparticles. This result however, is the first example of an orientation dependent trapping situation using only a TEM_00 beam. Typical experimental arrangements cannot determine much information on the axial position of a trapped particle relative to the trap focus; this result indicates not only that dimers can be trapped in multiple axial positions but also their trapping behaviour is heavily dependent on said axial position. As such it is necessary that positional information in the z-axis can be elucidated if multiple spheres are trapped simultaneously.

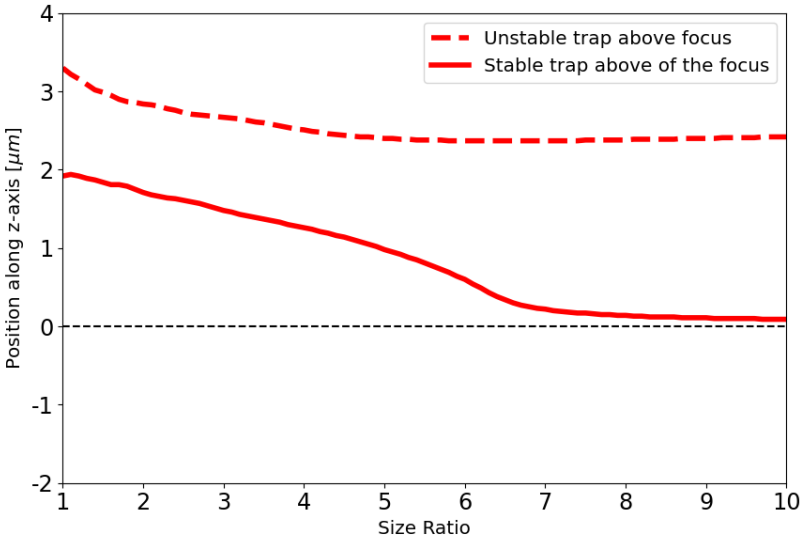

(a)

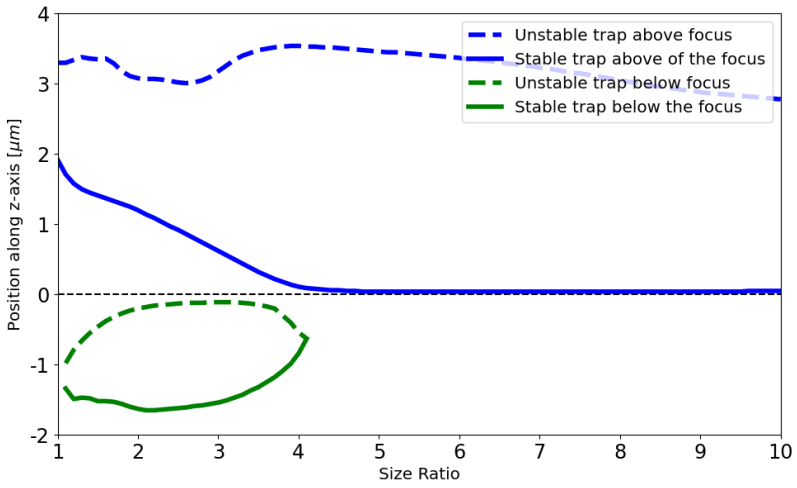

(b)

Figure 4.3: Equilibrium positions of optically trapped dimers with varying size ratio, dashed lines represent unstable traps whereas solid lines are for stable equilibrium positions. (a) shows that dimers while in their 'standard' orientation will always have a single equilibrium position. (b) shows that when the same dimer is in its' 'inverted' orientation can be trapped in two axial positions, one below the focus and one above the focus.

4.1.1 Non-trivial equilibrium configurations

Computing the equilibrium positions when a dimer is aligned with the electric field is relatively simple as the orientational torque is minimised (see Eq.**??**). Meaning once trapped the dimer is unlikely to change orientation enough to escape the trap. Regardless, that does not rule out the possibility that there is a stable configuration where the orientation not strictly vertical, in fact most experimental work with symmetric nano-dimers will trap them lying perpendicular to the beam direction [1, 17]. Unlike in Sec. 4.1 we cannot simply measure the optical force and torque as the parameter space is too large and determining if a particular position and orientation is stable is not clear based solely on force and torque measurements [6]. Using the same simulation parameters as before we ran a number short simulations (total simulation time was 0.005 s) with the laser power increased to 500 mW. Each simulation started with the dimer in a different starting position and orientation, due to the high laser power the dimers either escaped the trap or were stably trapped. The $z - \theta$ phase space - where θ is the angle between the direction of beam propagation and the dimer's orientation vector ($\theta = 0^\circ$ is the 'standard' orientation) - can be divided into different regions depending on which equilibrium configuration is reached.

Interestingly while the trap strength of these off-axis traps are similar in magnitude to the vertically aligned dimers, but when the laser power is lowered (around 5 mW) the traps become metastable; after reaching its equilibrium configuration the particle behaves similarly to a typically trapped dimer but the trapping potential is small enough that the dimer escapes in as little time as less than a second or after nearly a full 3 seconds. Running similar simulations but for vertical configurations sees the dimer remaining trapped, even after 30 seconds of run time, indicating that the trapping potential is far greater than the thermal energy. This suggests that the reason this off-axis configuration is metastable is due to the increased rotational freedom. Similar configurations have been explored with ellipsoids; Zhu *et al.* looked at the dynamics of various elliptical particles and found that regardless of shape or initial orientation the particle would tend towards either a purely vertical or purely horizontal orientation [28].

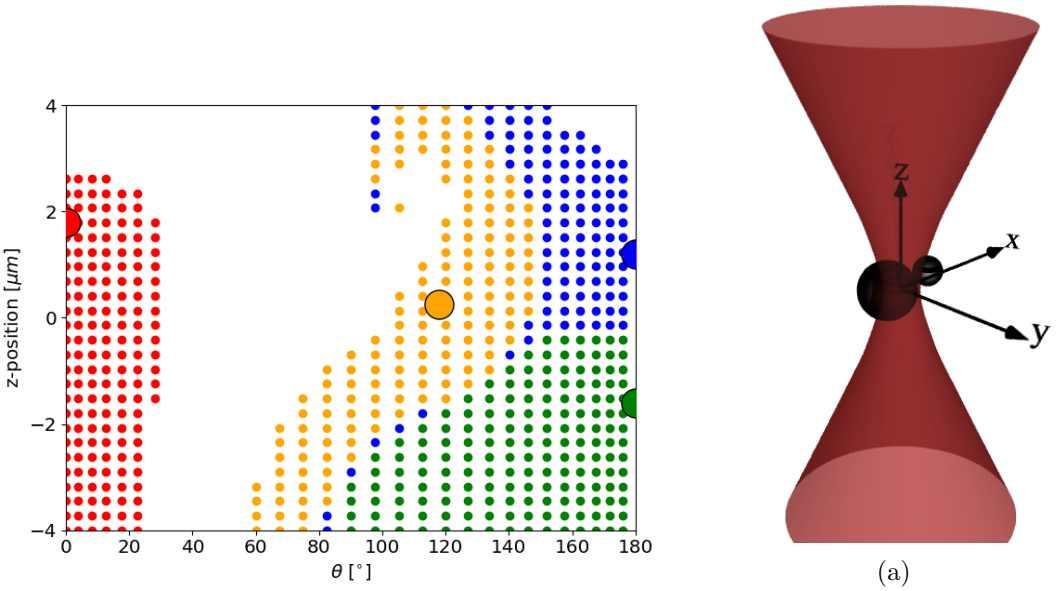

(a)

Figure 4.4: Map of $z - \theta$ phase space using a dimer of size ratio 2 with a laser power of 500 mW ($\theta = 0\circ$ is the 'standard' orientation and $\theta = 180°$ is the 'inverted' orientation). The stable configurations are indicated by the larger circles and the starting conditions are colour coded to match the stable point they end up in. Right hand render shows a dimer in its off-axis configuration.

4.2 Continuous rotational motion in circularly polarised light

One aspect that has yet to be covered in depth with regards to spherical aggregates of any construction is their interaction with circularly polarised light. For homogenous spheres the optical torque is regarded as being negligible as the spin density cannot impart angular momentum while propagating in a homogenous medium. Dimers however, have been shown to experience an optical torque [22, 1, 17] while trapped in a circular polarised beam. In our simulations we found that dimers would rotate about their long axis when trapped in circularly polarised light. In this section we want to discuss how this behaviour is influenced by size, position, and orientation; and furthermore, we wish to address possible explanations for this behaviour, as none of the current theories into optically induced rotation seem plausible.

4.2.1 Polarisation Dependency on Dimer trajectory

In their paper Vigilante *et al* attribute the rotational motion to the anisotropic shape of the dimer [22]. Anisotropic scattering is a viable theory for describing optical rotation, however there is usually an optical axis about which rotation occurs. For a dimer this is typically the orientation vector that passes through the centres of both spheres [1, 17, 4]. There have been cases where the particle's cross sectional shape is engineered to scatter light in one particular direction [9], but if this was the case then the dimer should rotate when illuminated by any polarisation of light.

To that end, we simulated the motion of an optically trapped dimer in beams of varying polarisation ($NA = 1.2$, $P = 100\ mW$), the dimer is composed of polystyrene ($n_p = 1.59$, $n_m = 1.33$). Each simulation was run for 1 second ($\Delta t = 10^{-}5$) and at the end we looked at the orientational time series; the dimer's orientation is recorded as a quaternion which can be easily converted to a 3-dimensional rotation matrix. By considering only the transverse components ($U_{1,x}$, $U_{1,y}$, $U_{2,x}$, & $U_{2,y}$) of the rotation matrix and taking the Fourier transformation of their time series reveals the rotational frequency. The laser power is set to 100 mW to avoid large thermal fluctuations and so that the Fourier series of the transverse components approximates $\delta(\omega_{rot} - f)$ - the Dirac delta function centred at the rotational frequency ω_{rot}.

$$\begin{aligned} q(t) \rightarrow R(t) &= \begin{pmatrix} U_{1,x}(t) & U_{2,x}(t) & U_{3,x}(t) \\ U_{1,y}(t) & U_{2,y}(t) & U_{3,y}(t) \\ U_{1,z}(t) & U_{2,z}(t) & U_{3,z}(t) \end{pmatrix} \\ &\rightarrow \int_{-\infty}^{\infty} R(t) e^{-i2\pi f t} dt = \begin{pmatrix} \delta(\omega_{rot} - f) & \delta(\omega_{rot} - f) & \delta(f) \\ \delta(\omega_{rot} - f) & \delta(\omega_{rot} - f) & \delta(f) \\ \delta(f) & \delta(f) & \delta(f) \end{pmatrix} \end{aligned} \tag{4.1}$$

If the rotational frequency was not immediately obvious the simulation was repeated but over a longer simulation time. Four different size ratio of dimers were studied, both in their 'standard' and 'inverted' orientations. The results of this are displayed in

Fig. 4.5:

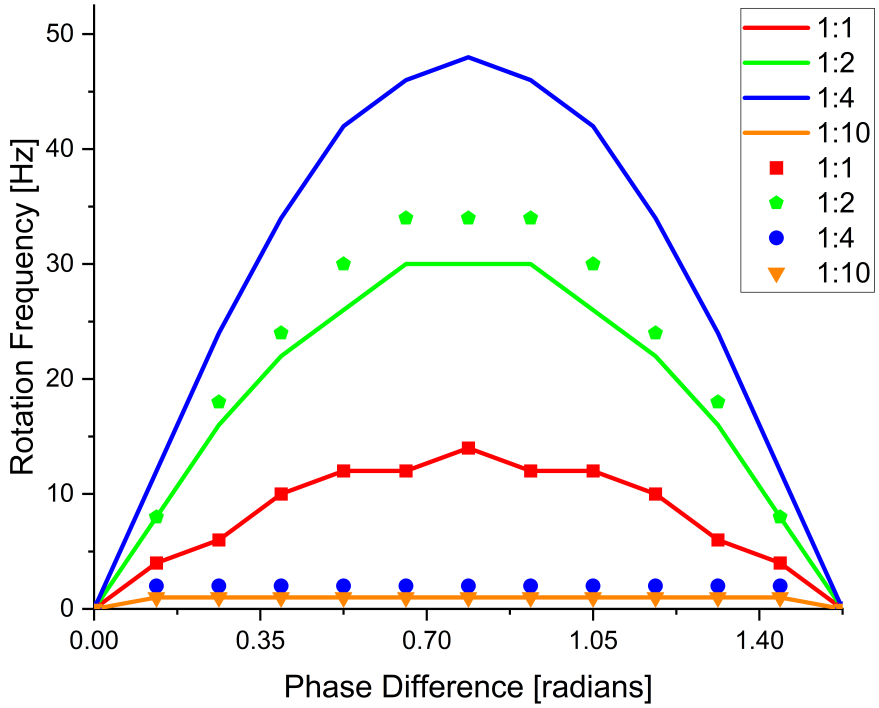

Figure 4.5: Rotation frequency vs component phase difference for differently sized dimers. The solid lines represent the rotation rate experienced while the dimer is in its standard orientation, whereas the solid points are for the case where the orientation is inverted. Laser power = 100 mW.

This shows us that these optical rotations are polarisation dependent and not merely an example of the dimer scattering light asymmetrically. We also know that this cannot be a similar mechanism to that of experimental works [1, 17] as in our simulations the dimer's long axis is parallel to the electric field. In this orientation the dimer's optical axis is aligned perpendicular to the polarisation vector meaning that there should be no angular momentum transferred along the optical axis. This is consistent with other experiments involving elongated particles. A dual beam trap was used to study the dynamics of "disk like" particles. They found that these particles had one of two stable orientations: Either orienting with the 'flat' side perpendicular to the beam trap, with

no rotation being observed [5]. Or orientating with the 'flat' side parallel to the trap, in which case the long axis was aligned with the polarisation vector and thus rotational motion was detected [5].

4.2.2 Brownian Vortex via Curl of Spin momentum

In their work Vigilante refers to the spin-curl effects demonstrated by Grier *et al* [18], in which the curl of the spin density leads to a second order optical force that orbits around the beams central axis [25]. While several papers have demonstrated this phenomena [26, 27, 23] it was only properly formalised by [18]. In which they showed that the seemingly random trajectory of a trapped sphere was biased by the polarisation state of the trapping beam. While not immediately evident from the trajectory the helicity of the trapping beam was revealed by computing the particle's probability flux using.

$$j(r) = \frac{1}{N-1}\sum_{j=1}^{N-1} \frac{r_{j+1} - r_j}{\tau} \delta_{sigma_j}\left(r - \frac{r_{j+1} + r_j}{2}\right) \tag{4.2}$$

where δ_{σ_j} is the kernel of an adaptive density estimator [21]. (4.2) describes the direction a trapped sphere is most likely move in given our statistical knowledge of the trajectories probability density function. A finite estimation of the density function $p(r)$ is used in [18].

$$p(r) = \frac{1}{N}\sum_{j=1}^{N} \delta_{\sigma_j}(r - r_j) \tag{4.3}$$

The probability flux reveals a biased motion in the trajectory of a single sphere (see Fig. 4.6). This biased motion results in a slight orbital motion about the central axis of the trapping beam, the orbital frequency is shown to be proportional to the polarisation state of the trapping beam.

While the results from [18] suggest that the optical rotation seen in asymmetric dimers can be attributed to the same spin-curl forces there are several questions that cannot be explained purely by the spin-curl force.

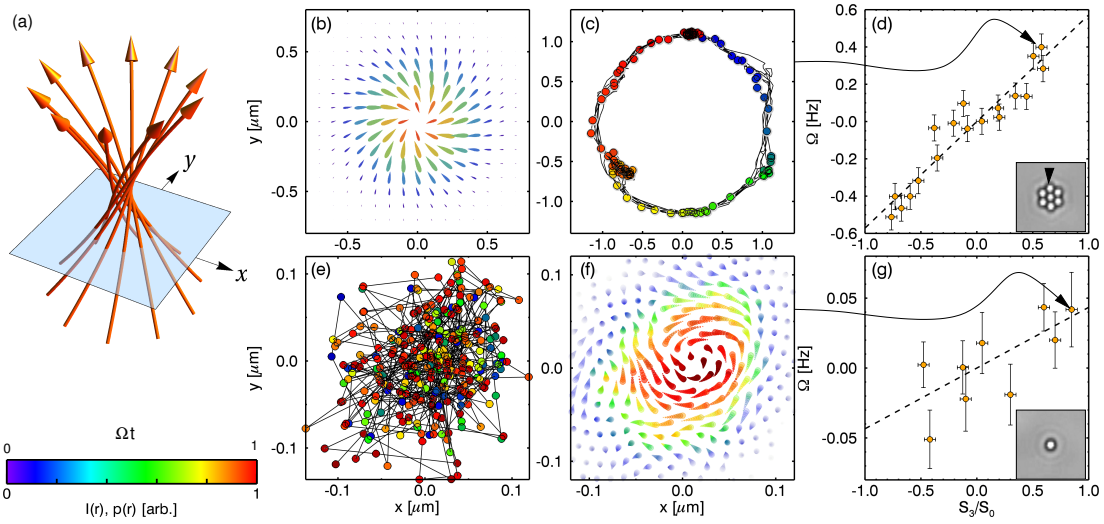

Figure 4.6: Figure reused from [18]. (a) shows how the momentum density of a Gaussian beam is twisted while using circularly polarised light. The top row (figures (b)-(d)) shows a 7 sphere cluster trapped in a circularly polarised beam. Due to the clusters asymmetric susceptibility to polarization the cluster rotates in the $x-y$ plane. Whereas the bottom row (figures (e) - (g)) show the similar results for a single sphere. In this instance the sphere does not rotate but instead orbits the beam axis. In both instances the motion is proportional to the degree of polarisation (see figures (d) and (g)) but for the single sphere this motion is only revealed when using (4.2) & (4.3). Reused with permission from author

4.2.3 Optical torque differences

In their paper Grier *et al* show that a 7 sphere cluster will rotate when trapped in circularly polarised light but a homogenous sphere will have a slight curl to its trajectory. They attribute this to the curl of the spin angular momentum generating a "Brownian vortex". But what is more interesting, and something that appears unaddressed, is how the effects of this vortex change based on the overall shape of the target particle.

You would not expect that the addition of a single additional sphere should drastically adjust the torque especially if said sphere is relatively small. However when we measured the optical torque of a single sphere and a dimer - $a_I/a_{II} = 10$ - we found the exact opposite. In both cases we used the same trapping beam as used for fig. 4.5 but with a circularly polarised beam. Both the sphere and dimer were rotated in the $x-z$ plane and the all three components of the optical torque were recorded.

The torques about the x and y axis can be somewhat understood as the second

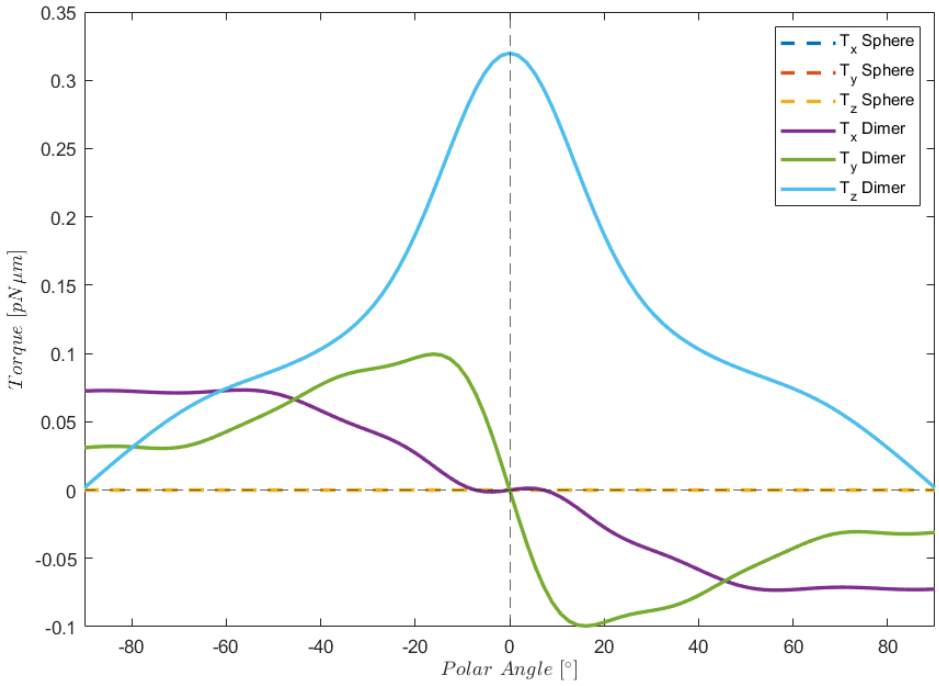

Figure 4.7: Optical toque experienced by a dimer ($a_I/aII = 10$) and a single isotropic sphere. Both were rotated in the $x - z$ plane and the angle between U_z and the beam axis gives the polar angle.The solid lines denote the torque experienced by the dimer whereas the dashed lines represent the torque experienced by the sphere.

sphere is being drawn back towards the centre of the trap by the gradient forces. The same cannot be said for the z- component of the optical torque, which is non-zero even at a 80° angle. This cannot be simply explained via spin-curl effects, as the 'Brownian vortex' should instead be driving the dimer around the beam axis - similar to how the 7 sphere cluster behaved. What is clear that the mere combination of two spheres results in a unique behaviour that has not been previously investigated.

4.2.4 Rotational frequency as a function of size ratio and orientation

One factor t Intuitively, you would expect that a larger particle would experience a greater torque and therefore rotate faster. By repeating the same kinds of simulation as used in 4.5 but for a circularly polarised beam $\phi = 90\circ$ it was found that not only is the rotation rate dependent on the size of the dimer, but also on its orientation and

therefore their axial position.

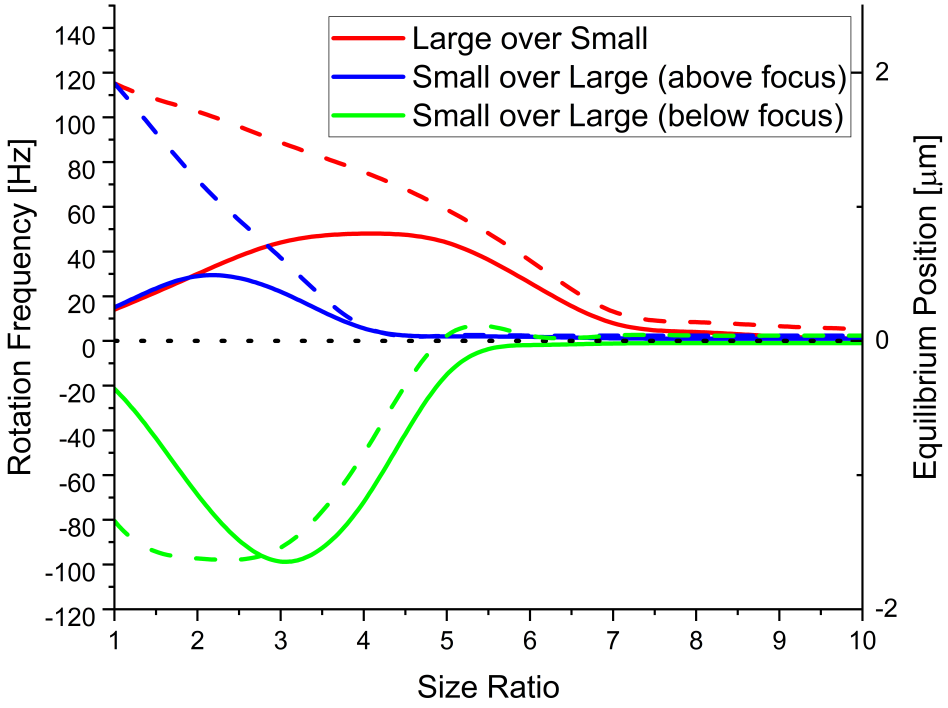

Figure 4.8: Rotation rate plotted against dimer size ratio while trapped in a circularly polarised beam; a positive rotation rate indicates clockwise rotation, whereas a negative rotation rate indicates counter-clockwise rotation. The red line is for the case of a dimer in its 'standard' orientation. The blue line is for the case when the dimer is in its 'inverted' orientation while trapped above the focus of the beam. And lastly the green line is for the case when the dimer is in its 'inverted' orientation, but when it is trapped below the focus of the beam.

It is difficult to see from the graph, but the rotation rate never truly goes down to zero, reaching a minimum of 2 Hz, which would imply that a second sphere of radius 200 nm is enough to induce rotational motion. What is also interesting is that the rotation rate is not correlated directly with either the particle size or the equilibrium position. This is in stark contrast to previous reports of dimer optical rotation; Ahn *et al.* reported that the rotational frequency is maximised when the dimer is symmetric [1]. Their work was conducted in a vacuum so the only limiting factor to the optical

rotational motion is the structural stability of the particle itself.

4.2.5 Gyroscopic Precession using asymmetric dimers

As mentioned in section 4.1.1 for specificity sized dimers there is the potential for non-vertical trapping orientations in which the dimer is still stably trapped. When a circularly polarised beam is used the dimer exhibits gyroscopic precession. As shown in fig. 4.9 the dimer's trajectory exhibits periodic rotation, both around its long axis and about the beam axis.

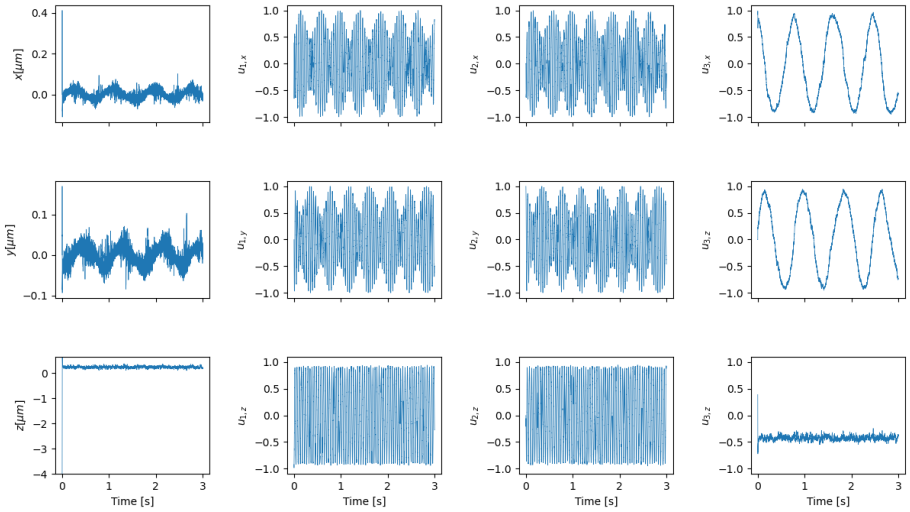

Figure 4.9: 3 second trajectory of a dimer ($a_I/a_{II} = 2$) trapped in an off axis orientation with a circularly polarised beam ($P = 100\,mW$). The far left column depicts the dimer's centre of mass position with time; the remaining 3 columns show the 9 components of the dimers' rotation matrix, with each column being associated with one of its three principal axis.

Applying a Fourier analysis to the above trajectory reveals the 3 fundamental frequencies typically associated with gyroscopic precession. Fig. 4.10 gives a representative idea of the motion seen in fig. 4.9. Firstly there is precession, is denoted by ψ, this causes the dimer to rotate in the XY plane while maintaining a constant polar angle. The precession can be due to the dimer having inhomogeneous polarisation susceptibility. Since its long axis is more susceptible to being polarised the dimer will try to

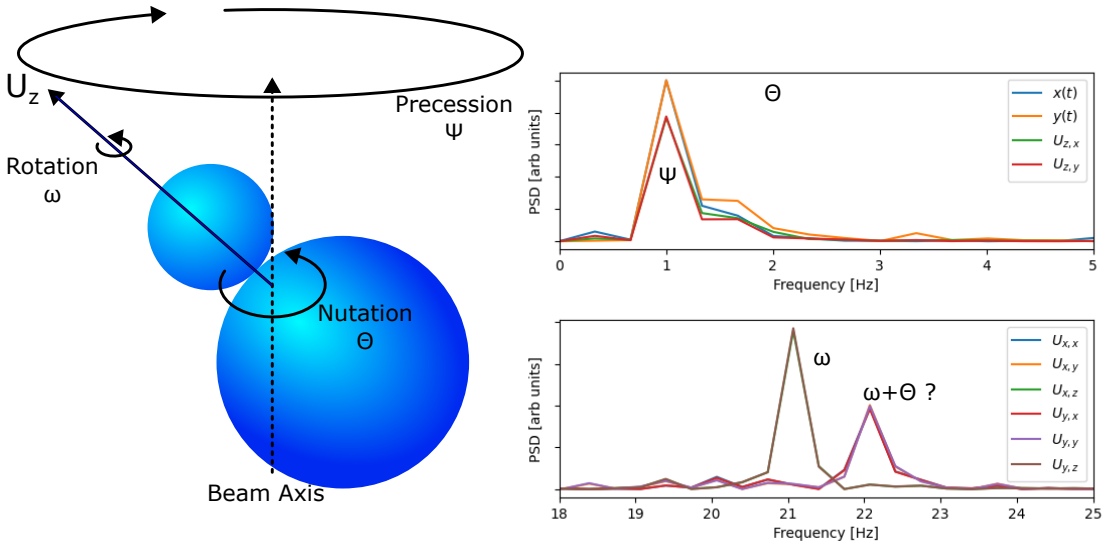

Figure 4.10: Representative diagram of the gyroscopic precession from fig. 4.9. The dimer has three principal angular frequencies: The rotation (ω) occurs around the the dimer's long axis. Precession (ψ) is seen where the dimer rotates around the beam axis. Nutation (θ) is due to the dimer's centre of diffusion orbiting the beam axis. Shown on the right is the power spectra from fig. 4.9 with the associated frequencies labelled. The power spectrum have been zoomed in on the relevant frequencies to highlight the precise values.

align its long axis with the polarisation vector [4]. Second there is nutation, denoted by θ, which is due to the dimer's Brownian motion being influenced by the 'Brownian vortex', as predicted by [18]. And lastly there is rotation, denoted by ω, where the dimer spins around its long axis as it did in 4.2.1 & 4.2.4.

What is interesting is that while we see the precession and nutation also contribute to the rotation frequency. As can be seen in both fig. 4.9 and fig. 4.10 the rotation matrix components $U_{x,x}$, $U_{x,y}$, $U_{y,x}$ and $U_{y,y}$

This gyroscopic motion has been demonstrated previously in nanoparticles [28, 16, 10, 11] but has not been observed for micron scale aggregates. What is interesting that the precession is seen around the particle's optical axis (in the case of a dimer this would be its long axis). Fig. 4.9 instead shows the precession occurring perpendicular to the optical axis. In the former case the precession can be explained as simply occurring due to the reaction torque from the surrounding fluid [28]. In their analysis of ellipsoidal particles, Zhu *et al.* found that when the particle rotated around their minimal inertial

axis (similar to the observed behaviour in dimers), the particle would quickly 'stabilise' by aligning its' optical axis with the beam axis. This highlights that a spherical dimer is capable of rotating about its minimal inertial axis while remaining stably trapped. This has potential implications beyond simply understanding particle dynamics.

Further analysis of the mechanism behind the precession of off-axis dimers may provide insights into controlling Brownian motion. An experimental work trying to 'cool' nano-dimers by controlling the motion in all 6 degrees of freedom found that even while the rotation about the short axis' could be controlled the free rotation around the dimers' long axis resulted in an unpredictable torsional vibration [2]. Understanding how rotational motion arises in the Mie-regime could allow researchers to build a robust theoretical framework to construct beam structures that eliminate any unwanted rotational motion from a target particle. Conversely, the same framework could allow for precise measurements of the optical torque applied to a target particle, allowing for characterisation of complex shaped particles' interactions with an optical trap.

4.3 Characterisation of asymmetric dimers via PSD analysis

As discussed in **??**, one of the methods developed to work in conjunction with [22] is a simulated quadrant photo diode for as a position detection system. While it is possible to extract all of the relevant dynamical information from a simulation, confirming the same behaviour in an experimental setting can be challenging if dealing with a non-birefringent anisotropic scatterer. The QPD is composed of 4 photodiodes that measure the intensity of light incident on their surfaces. Using *ott* we can define a region in the far-field that is analogues to the surface of the QPD surface. Evaluating the electric field across this surface gives us an approximation of the QPD signal outputted in an experimental situation. This does not provide a one-to-one result however as hardware errors (i.e. internal resistance, external light sources, and vibrations) would distort the signal somewhat. We can use this as a means to examine the limitations of using back-focal plane interferometry as a means for characterising anisotropic scatterers.

As a benchmark we start by considering a single sphere within an optical trap. A single polystyrene sphere suspended in water ($a = 1\mu m$, $n_p = 1.59$, $n_m = 1.33$) was trapped by a focused Gaussian beam ($NA = 1.25$) using circularly polarised light. For the sake of time efficiency the trajectory was sampled every 10 time steps, meaning the upper bound on the power spectra is $f_{Nyq} = f_{sample}/2 = 5000\ Hz$. To optimise the frequency window we fitted the power spectra using the aliased Lorentzian (Eq. (**??**)).

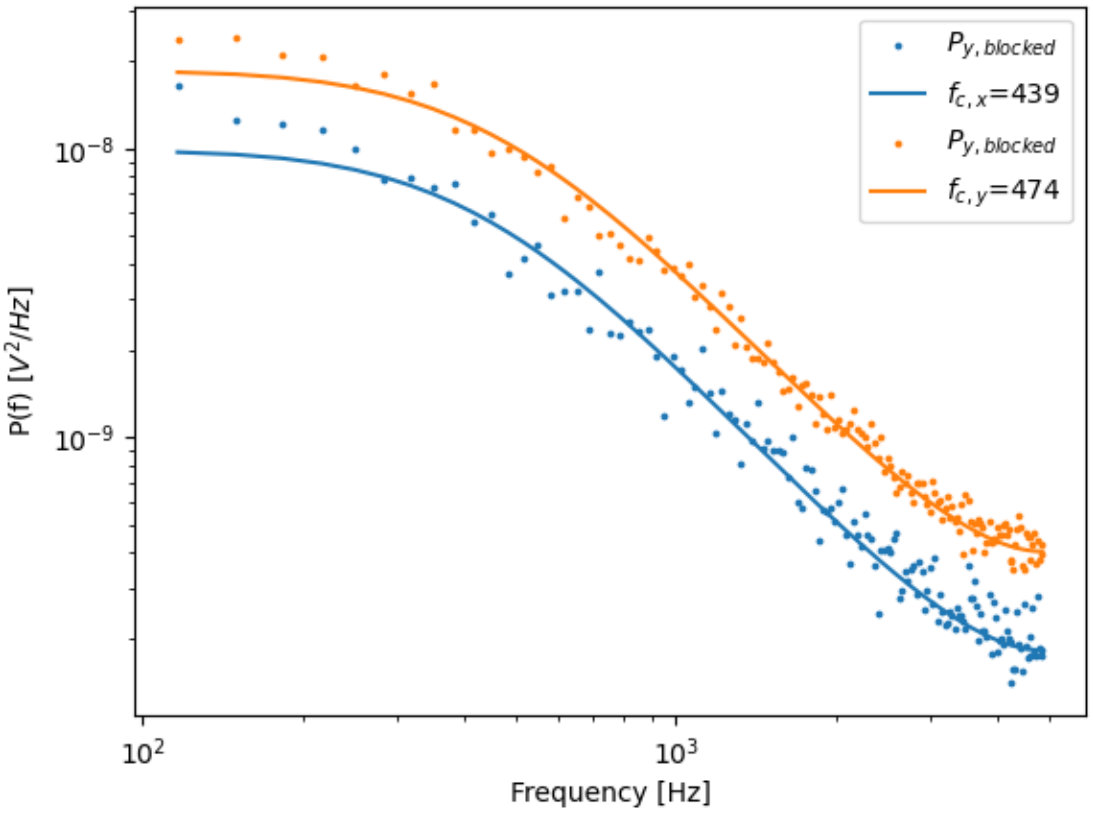

Figure 4.11: Recorded power spectra fitted to eq. **??**, scattered points represents the blocked data ($n_b = 100$). Corner frequency for the Lorentzian curves are reported in the legend.

As shown in fig. 4.11, the two power spectra report different corner frequencies which would be indicate that the trap is not perfectly circular. We can use both *ott* and the trajectory itself to derive an estimation of the trap geometry. The corner frequencies and corresponding trap stiffness are reported below:

Table 4.1: QPD fitting for single sphere

Fitting parameter	*ott* estimates		QPD fitting		Trajectory fitting	
f_c $[Hz]$	447	450	439	474	523	513
$\sigma(f_c)$ $[Hz]$	—	—	9.30	9.65	8.67	8.61
κ $[pN/\mu m]$	53.05	53.40	51.96	56.09	61.94	60.7
Ellipticity	8.16 %		27.17 %		13.8 %	

Where $\sigma(f_c)$ is computed from [3], where the variance is based upon our choice of frequency boundaries ($f_{min} : f_{max} = 100\ Hz : 5000\ Hz$). And the ellipticity of the beam is given by $e = (1 - \kappa_y/\kappa_x)^{0.5}$ and is a measure of the symmetry of the beam wavefront. Its clear from these initial results that the QPD is more sensitive to changes along the y-axis than the x-axis when compared to the direct *ott* calculations. This is somewhat reflected in the trajectory results. Typically, even an industrial Gaussian beam will produce an elliptical diffraction limit spot when heavily focused; in their tutorial for optimizing the PSD analysis, Berg and Sorensen reported a ellipticity of around 15 % after a total calibration time of 80 seconds [3].

The reason for the discrepancies between all 3 methods is due to what is actually being measured. The *ott* estimates are simply looking at the differences in the trapping strength along the Cartesian axis'. If calibrated over an long enough time frame you would expect that the resulting power spectra would exactly mirror the *ott* predictions. However over a short calibration time a QPD will only sample a small trajectory that does not fully explore the trapping plane. There is a clear trade off in terms of accuracy and computation time as shorter calibration runs are computationally more efficient but prone to errors. This is the case even if we know the exact positional data.

With this in mind, let us consider a symmetric dimer that is optically trapped by the same Gaussian beam. Not only does the dimer's equilibrium position change but it is subjected to rotational motion due to its unequal moments of inertia. This is reflected in the calibration results using the simulated QPD, where we see a drastically different estimation between the *ott* estimate and the QPD estimate.

Table 4.2: QPD fitting for symmetric dimer

Fitting parameter	*ott* estimate		QPD fitting		Simulation fitting	
f_c $[Hz]$	409	334	431	424	274	285
κ $[pN/\mu m]$	48.51	39.58	51.13	50.26	32.45	33.75
Ellipticity	42.8 %		12.7 %		13.8 %	

Now we see that the *ott* predicts a more elliptical trap compared to the QPD model which says the trap is far more symmetrical while trapping a symmetric dimer. A potential reason that *ott* no longer expects a circular trap could be due to how it computes the beam shape coefficients; by point matching in the far field before the focus means a loss in accuracy for objects that trap above the focus. The change in the QPD estimation can be partially explained by the fact that rotational effects are not accounted for in the Lorentzian power spectra, only translational motion. Typically, rotational motion is only ever detected when it is periodic (take for example Fig. **??**), when the motion is stochastic the entire power spectra is effected making it near impossible to separate the translational and rotational contributions from a single power spectra.

4.4 Conclusions

Considering the simplicity of a scatterer such as a dimer, one would assume that the dynamics of such an object would be relatively easy to predict. Simulations of dimers in the Mie regime show that not only do they have multiple positions and orientations in which they can be trapped but also that their interaction with circularly polarised light is heavily dependent on the axial position and trapping orientation.

Dimer's have the potential to be used as tunable micro-rotors, being simple to synthesise and can be made out of any material of choice. The rotation demonstrated by dimer's is not accurately described in previous literature which raises questions on the interactions between circularly polarised light and spherical aggregates. Until now, our understanding of angular momentum transfer has been either focused on single particles (where momentum transfer is easily described by Lorenz-Mie theory) or for large aggregates of particles, where the angular momentum transfer between individual particles is not considered. This could provide a greater understanding of angular

momentum and help in the development of better torque sensing or torque preventing methods.

Conventional calibration methods will not be adequate however, while angular motion can be detected using complicated set ups [2], this can only provide an estimate of the magnitude of a particle's angular motion. This is perfectly fine in cases where the rotational motion is stochastic and intuitively predictable (i.e. a dimer in a vertical orientation undergoing stochastic Brownian motion), but in the case the the motion is instead periodic characterising it requires instantaneous measurements of the particle's motion.

Bibliography

[1] Jonghoon Ahn, Zhujing Xu, Jaehoon Bang, et al. "Optically Levitated Nanodumbbell Torsion Balance and GHz Nanomechanical Rotor". In: *Physical Review Letters* 121.3 (July 2018), p. 033603. ISSN: 1079-7114. DOI: 10.1103/physrevlett.121.033603.

[2] Jaehoon Bang, T. Seberson, Peng Ju, et al. "Five-dimensional cooling and nonlinear dynamics of an optically levitated nanodumbbell". In: *Physical Review Research* 2.4 (Oct. 2020), p. 043054. ISSN: 2643-1564. DOI: 10.1103/physrevresearch.2.043054.

[3] Kirstine Berg-Sørensen and Henrik Flyvbjerg. "Power spectrum analysis for optical tweezers". In: 75 (2004), pp. 594–612. ISSN: 0034-6748. DOI: 10.1063/1.1645654.

[4] Graham D. Bruce, Paloma Rodríguez-Sevilla, and Kishan Dholakia. "Initiating revolutions for optical manipulation: the origins and applications of rotational dynamics of trapped particles". In: *Advances in Physics: X* 6.1 (Dec. 2020). ISSN: 2374-6149. DOI: 10.1080/23746149.2020.1838322.

[5] Oto Brzobohatý, Alejandro V. Arzola, Martin Šiler, et al. "Complex rotational dynamics of multiple spheroidal particles in a circularly polarized, dual beam trap". In: *Optics Express* 23.6 (Mar. 2015), p. 7273. ISSN: 1094-4087. DOI: 10.1364/oe.23.007273.

[6] Ann A.M. Bui, Alexander B. Stilgoe, Isaac C.D. Lenton, et al. "Theory and practice of simulation of optical tweezers". In: *Journal of Quantitative Spec-*

troscopy and Radiative Transfer 195 (July 2017), pp. 66–75. ISSN: 0022-4073. DOI: 10.1016/j.jqsrt.2016.12.026.

[7] M. Capitanio, G. Romano, R. Ballerini, et al. "Calibration of optical tweezers with differential interference contrast signals". In: *Review of Scientific Instruments* 73.4 (Apr. 2002), pp. 1687–1696. ISSN: 1089-7623. DOI: 10.1063/1.1460929.

[8] Chetana D, Praveen P, Nagesh B V, et al. "Laser polarization driven micromanipulation and reorientation dynamics of an asymmetric shaped microscopic biomaterial using optical tweezers". In: *Journal of Optics* 24.9 (Aug. 2022), p. 094007. ISSN: 2040-8986. DOI: 10.1088/2040-8986/ac868c.

[9] E. Higurashi, H. Ukita, H. Tanaka, et al. "Optically induced rotation of anisotropic micro-objects fabricated by surface micromachining". In: *Applied Physics Letters* 64.17 (Apr. 1994), pp. 2209–2210. ISSN: 1077-3118. DOI: 10.1063/1.111675.

[10] Thai M. Hoang, Yue Ma, Jonghoon Ahn, et al. "Torsional Optomechanics of a Levitated Nonspherical Nanoparticle". In: *Physical Review Letters* 117.12 (Sept. 2016), p. 123604. ISSN: 1079-7114. DOI: 10.1103/physrevlett.117.123604.

[11] Stefan Kuhn, Alon Kosloff, Benjamin A. Stickler, et al. "Full Rotational Control of Levitated Silicon Nanorods". In: (2016). DOI: 10.48550/ARXIV.1608.07315.

[12] Martin Li and Jochen Arlt. "Trapping multiple particles in single optical tweezers". In: 281 (2008), pp. 135–140. ISSN: 0030-4018. DOI: 10.1016/j.optcom.2007.09.032.

[13] J. Loudet, B. M. Mihiretie, and B. Pouligny. "Optically driven oscillations of ellipsoidal particles. Part II: Ray-optics calculations". In: 37 (2014). ISSN: 1292-8941. DOI: 10.1140/epje/i2014-14125-y.

[14] P. Praveen, Yogesha, Shruthi S. Iyengar, et al. "Two particle tracking and detection in a single Gaussian beam optical trap". In: 55 (2016), p. 585. ISSN: 0003-6935. DOI: 10.1364/ao.55.000585.

[15] Antonio Alvaro Ranha Neves and Carlos Lenz Cesar. "Analytical calculation of optical forces on spherical particles in optical tweezers: tutorial". In: *Journal of the Optical Society of America B* 36.6 (Mar. 2019), p. 1525. ISSN: 1520-8540. DOI: 10.1364/josab.36.001525.

[16] Muddassar Rashid, Marko Toroš, Ashley Setter, et al. "Precession Motion in Levitated Optomechanics". In: *Physical Review Letters* 121.25 (Dec. 2018), p. 253601. ISSN: 1079-7114. DOI: 10.1103/physrevlett.121.253601.

[17] René Reimann, Michael Doderer, Erik Hebestreit, et al. "GHz Rotation of an Optically Trapped Nanoparticle in Vacuum". In: *Physical Review Letters* 121.3 (July 2018), p. 033602. ISSN: 1079-7114. DOI: 10.1103/physrevlett.121.033602.

[18] David B. Ruffner and David G. Grier. "Optical Forces and Torques in Nonuniform Beams of Light". In: *Physical Review Letters* 108.17 (Apr. 2012), p. 173602. ISSN: 1079-7114. DOI: 10.1103/physrevlett.108.173602.

[19] V. Shahabadi and E. Madadi. "Effective multiple optical trapping of sub-micrometer particles with petal beams". In: *Journal of the Optical Society of America B* 37.12 (Nov. 2020), p. 3665. ISSN: 1520-8540. DOI: 10.1364/josab.402944.

[20] Xu Sheng-Hua, Li Yin-Mei, Lou Li-Ren, et al. "Computer simulation of the collision frequency of two particles in optical tweezers". In: 14 (2005), pp. 382–385. ISSN: 1009-1963. DOI: 10.1088/1009-1963/14/2/028.

[21] B.W. Silverman. *Denisty Estimation for Statistical and Data Analysis*. Chapman and Hall, 1986.

[22] Wyatt Vigilante, Oscar Lopez, and Jerome Fung. "Brownian dynamics simulations of sphere clusters in optical tweezers". In: *Optics Express* 28.24 (Nov. 2020), p. 36131. ISSN: 1094-4087. DOI: 10.1364/oe.409078.

[23] Xi-Lin Wang, Jing Chen, Yongnan Li, et al. "Optical orbital angular momentum from the curl of polarization". In: *Physical Review Letters* 105.25 (Dec. 2010), p. 253602. ISSN: 1079-7114. DOI: 10.1103/physrevlett.105.253602.

[24] Shenghua Xu, Yinmei Li, and Liren Lou. "Axial optical trapping forces on two particles trapped simultaneously by optical tweezers". In: 44 (2005), p. 2667. ISSN: 0003-6935. DOI: 10.1364/ao.44.002667.

[25] Aaron Yevick, Daniel J. Evans, and David G. Grier. "Photokinetic analysis of the forces and torques exerted by optical tweezers carrying angular momentum". In: *Philosophical Transactions of the Royal Society A: Mathematical, Physical and Engineering Sciences* 375.2087 (Feb. 2017), p. 20150432. ISSN: 1471-2962. DOI: 10.1098/rsta.2015.0432.

[26] Yiqiong Zhao, J. Scott Edgar, Gavin D. M. Jeffries, et al. "Spin-to-Orbital Angular Momentum Conversion in a Strongly Focused Optical Beam". In: *Physical Review Letters* 99.7 (Aug. 2007), p. 073901. ISSN: 1079-7114. DOI: 10.1103/physrevlett.99.073901.

[27] Yiqiong Zhao, David Shapiro, David Mcgloin, et al. "Direct observation of the transfer of orbital angular momentum to metal particles from a focused circularly polarized Gaussian beam". In: *Optics Express* 17.25 (Dec. 2009), p. 23316. ISSN: 1094-4087. DOI: 10.1364/oe.17.023316.

[28] Qi Zhu, Nan Li, Heming Su, et al. "Dynamic Analysis and Simulation of an Optically Levitated Rotating Ellipsoid Rotor in Liquid Medium". In: *Photonic Sensors* 12.2 (Sept. 2021), pp. 105–116. ISSN: 2190-7439. DOI: 10.1007/s13320-021-0639-0.